Synthesis, Structural Characterization and Phosphorescence Properties of Trigonal Zn(II) Carbene Complexes

Stefan Koop,[a] Ondřej Mrózek,[a] Lars Janiak,[a] Andrey Belyaev,[a] Markus Putscher,[b] Christel M. Marian,[b] and Andreas Steffen*,[a]*

[a] Department of Chemistry and Chemical Biology, TU Dortmund University

Otto-Hahn-Str. 6, 44227 Dortmund (Germany)

[b] Institute of Theoretical and Computational Chemistry, Heinrich Heine University Düsseldorf, 40225 Düsseldorf, Germany

E-mail: Christel.Marian@hhu.de, andreas.steffen@tu-dortmund.de

ABSTRACT

The sterically demanding *N*-heterocyclic carbene ITr (*N*,*N*′-bis(triphenylmethyl)imidazolylidene) was employed for the preparation of novel trigonal zinc(II) complexes of the type [ZnX_2(ITr)] (X = Cl (**1**), Br (**2**), I (**3**)), for which the low coordination mode was confirmed in both solution and the solid state. Because of the atypical coordination geometry, the reactivity of **1**-**3** was studied in

detail, using partial or exhaustive halide exchange and halide abstraction reactions to access [ZnLCl(ITr)] (L = carbazolate (**4**), 3,6-di-tert-butyl-carbazolate (**5**), phenoxazine (**6**) and phenothiazine (**7**)), [Zn(bdt)(ITr)] (bdt = benzene-1,2-dithiolate) (**8**) and cationic [Zn(μ_2-X)(ITr)]$_2$[BPh$^F_4$]$_2$ (X = Cl (**9**), Br (**10**), I (**11**)), all of which were isolated and structurally characterized. Importantly, for all complexes **4**-**11**, the trigonal coordination environment of the Zn^{II} ion is maintained, demonstrating a highly stabilizing effect due to the steric demand of the ITr ligand, which protects the metal center from further ligand association. In addition, complexes **1**-**3** and **8**-**11** show long-lived luminescence from triplet excited states in the solid state at room temperature according to our photophysical studies. Our quantum chemical DFT/MRCI calculations reveal that the phosphorescence of **8** originates from a locally excited triplet state on the bdt ligand. They further suggest that the phenyl substituents of ITr are photochemically not innocent but can coordinate to the electron deficient metal center of this trigonal complex in the excited state.

INTRODUCTION

Zinc, as a central metal, presents a plethora of advantageous properties making its coordination/organometallic complexes attractive candidates for many applications, including the utilization of organozinc species in organic synthesis or catalysis.[1] Moreover, zinc(II) complexes have recently received increased scientific attention as photoactive materials that can efficiently form luminescent or dark triplet excited states.[2–4] Particularly promising appears to be photoluminescent Zn^{II}/carbene systems for which efficient generation of long-lived phosphorescence and thermally activated delayed fluorescence were recently demonstrated.[4,5]

Among the most significant benefits a high abundance of 75 ppm in the earth's crust (comparable to Cu, Ce or Zr, for instance)[6] makes zinc widely available and cheap. Although a handful of reactive Zn^{I} molecules are known, e.g., cyclopentadienyl complexes of the type [(Cp*)ZnZn(Cp*)][7], the most common oxidation state of zinc is 2+. Besides excellent redox stability, the Zn^{II} center features a d^{10} electron configuration, which is beneficial for developing photoactive and photoluminescent complexes, as d^{10} systems lack metal-centered states through which excited states typically decay in a fast and non-radiative fashion.[8] Zn^{II} as a central metal also shows substantial variability of coordination modes (Figure 1A). While high-coordinated species, such as tetra-, penta-, and hexa-coordinated complexes, are prevalent among mononuclear complexes (98% of the overall scope according to the CCDC database, April 2023), achieving low-coordination modes becomes increasingly challenging due to higher reactivity. This difficulty reflects a strong tendency of the Zn^{II} center to compensate for its electron deficiency in low coordination modes. Despite their rareness, zinc complexes with coordination numbers two and three are highly desired molecules due to increased Lewis acidity, atypical reactivity or planar geometric configuration.

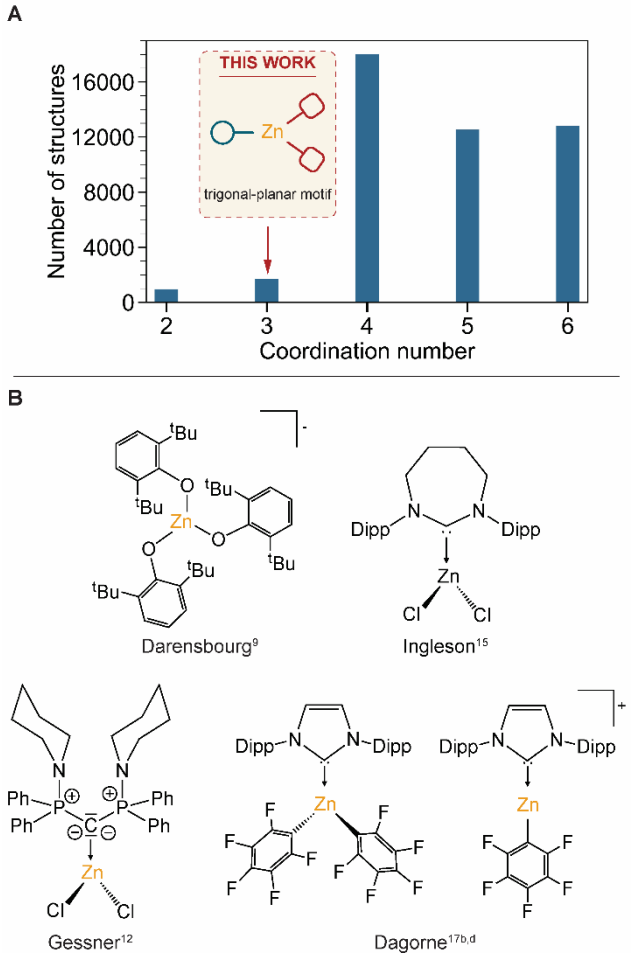

Figure 1. Number of structurally characterized Zn^{II} complexes with different coordination numbers (**A**) and selected examples of literature-known trigonal planar Zn^{II} molecules (**B**).

Low-coordination modes of Zn^{II} require a specific environment around the central metal consisting of very strongly σ-donating and sufficiently sterically demanding ligands. The former stabilizes complexes thermodynamically by compensating/lowering the electron-deficient character of the Zn^{II} center, while the latter ensures the protection of the metal from the attachment of additional ligands (such as molecules of solvent) and the increase of the coordination number, providing thus kinetic stabilization. Homoleptic trigonal planar complexes of the type $[Zn(E)_3]^-$,

where E = aryl-, alkoxide- or thiolate-based ligands (Figure 1B), have been known for more than two decades.[9,10] Although some of these compounds were tested as catalysts in the copolymerization of CO_2 with cyclohexane oxide or polymerization of epoxide, the usage and potential of this structural type is somewhat limited due to the rigid coordination sphere which prevents further chemical modification and modulation of chemical, physical or catalytic properties.[9] The direct reaction between $ZnCl_2$ and various C-donors (L) is a well-established synthetic pathway for preparing $ZnCl_2$:L adducts.[11,12] Depending on the character of the ligand L and the used solvent, a monomeric or dimeric arrangement can be obtained. Typically, dimeric species are formed upon solvent exclusion with coordinating properties or by using not sterically hindering ligands.[13,14] For C-donors with slightly increased bulk, monomeric (solvent-coordinated) molecules might be obtained in the presence of coordinating solvent (most commonly THF). In these two scenarios, the Zn^{II} metallic center maintains an archetypal coordination number of four. However, bypassing this behavior of zinc complexes, several recent articles reported the stabilization of rare trigonal planar molecules by employing very strong and bulky C-donors (Figure 1B).

Recently, Gessner and co-workers reported a spectacular ligand, di(amino) carbodiphosphorane (CDP'), with powerful C-donating properties, capable of stabilizing the trigonal planar motif upon coordination to the $ZnCl_2$ unit (Figure 1B).[12] Ingleson and co-workers reported that tri-coordinated zinc(II) complexes (Figure 1B) are accessible using stabilization provided by 7-Dipp (1,3-bis(2,6-diisopropylphenyl)-4,5,6,7-tetrahydro-1H-1,3-diazepin-3-ium-2-ide).[15] This comprehensive study showed that besides the parent molecule [Zn(7-Dipp)$(Cl)_2$], also further congeners, bearing, e.g., alkynyl, H- or THF ligands, can be isolated. A high degree of structural variability associated with low-coordinated Zn^{II} molecules stabilized by different N-

heterocyclic carbenes (NHC) is further demonstrated by recent works of Mondal et al. and Gour et al., who prepared trigonal-planar Zn^{II} complexes using fluorenyl-substituted NHC and six-membered NHC, respectively.[16] Another important class of low-coordinated Zn^{II} complexes bearing NHC ligands represents neutral di-organyl compounds of the type [Zn(NHC)(R_2)], first reported by Arduengo et al. and comprehensively studied by Dagorne and co-workers (Figure 1B).[17] These complexes, stable under an inert atmosphere, are readily accessible in high yields by adding the respective NHC to the ZnR_2 precursor offering a straightforward source of trigonal planar zinc(II) molecules. Another advantage is an easy modification of the coordination sphere using alkyl ligand abstraction or exchange to give additional trigonal planar derivatives or even two-coordinated complexes (Figure 1B).

The principal goal of this work is to explore the chemical and photophysical properties of trigonal planar complexes of Zn^{II} bearing a bulky N-heterocyclic carbene. Low-coordinated, photoluminescent compounds based on Zn^{II} have been mostly overlooked in the literature. However, their exploration appears relevant as some low-coordinated carbene complexes with a d^{10} electron configuration feature exceptionally high photoluminescence performance.[18]

RESULTS AND DISCUSSION

Synthesis and structural characterization of [ZnX_2(ITr)]

Our exploration of low-coordinated carbene zinc(II) halide complexes was initiated by the equimolar reaction between the in-situ deprotonated form of 1,3-bis(trityl)imidazolium tetrafluoroborate[19–21], ITr, with ZnX_2 (X = Cl, Br, I) (Figure 2A). After the work-up, the desired monomeric complexes [ZnX_2(ITr)] (X = Cl (**1**), Br (**2**), I (**3**)) were isolated in moderate yields

(~60%) and characterized by multinuclear NMR spectroscopy in THF-d_8 solutions. The ^{1}H spectra of **1-3** show one set of sharp signals corresponding to the ITr ligand coordinated to a ZnX_2 unit of C_s symmetry, while the $^{13}C\{^1H\}$ spectra reveal a resonance for the $C^{carbene}$ with a chemical shift of ~175 ppm that is considerably shifted upfield compared to free ITr (225.8 ppm)[19] and thus clearly proves the successful coordination to the metal center.

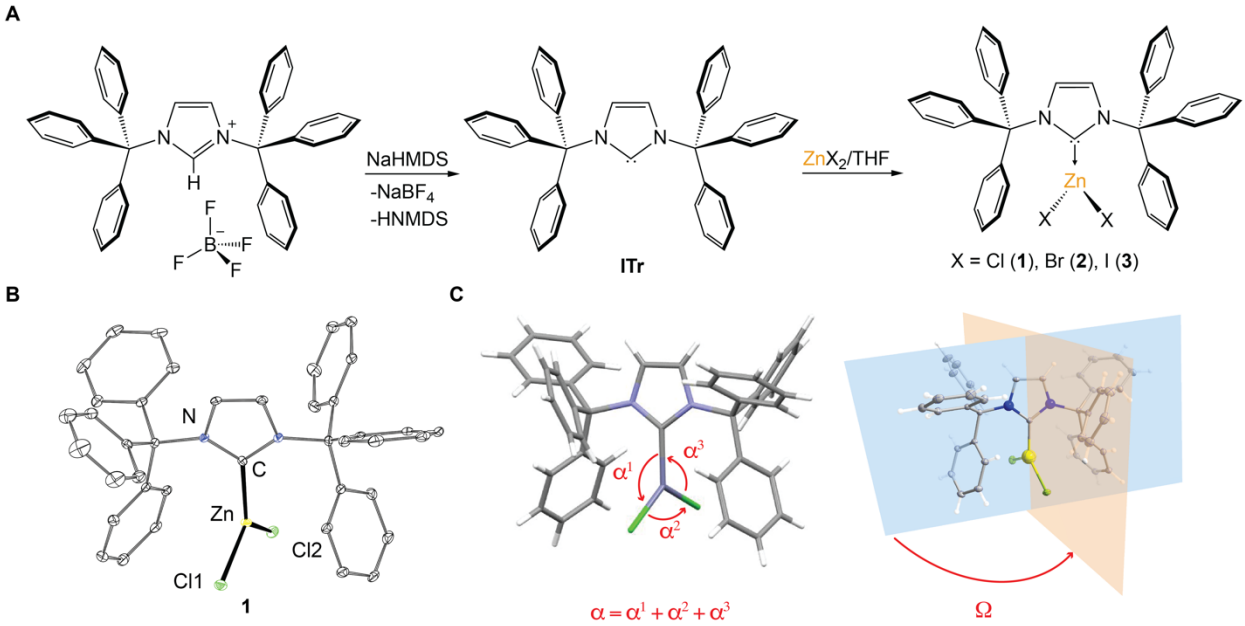

Figure 2. Synthesis of ITr complexes **1-3** (**A**), the molecular structure of **1** obtained by single crystal X-ray diffraction (**B**), and definition of angles α and Ω (**C**). Thermal ellipsoids are drawn at a 30% probability level, and hydrogen atoms together with co-crystallized molecules of toluene are omitted for clarity.

Single crystals suitable for X-ray diffraction analysis were obtained by diffusion of toluene as an anti-solvent to a solution of **1-3** in THF. All compounds crystallize in a monoclinic $P2_1/n$ space

group with four co-solvent molecules of toluene in a unit cell. The zinc(II) center of **1**-**3** exhibits a distorted trigonal planar coordination environment as evidenced by values of angle α (for definition see Figure 2C) close to 360º (Table 1). The Zn–X bond distances of **1**-**3** are in the range of those reported for tetra-coordinated zinc(II) halide complexes and trigonal-planar compounds of Zn^{II}.[11,12,15][14] For instance, the Zn–Cl bonds of 2.2170(5) and 2.2022(5) Å (Table 1) of **1** are only slightly shorter than observed for solvent-coordinated [$ZnCl_2$(IMes)(THF)][11] (2.2338(6) and 2.2344(7) Å) and CDP'-stabilized trigonal [ZnX_2(CDP)'] shown in Figure 1B (2.222(1) and 2.227(1) Å).[12] In addition, the Zn–$C^{carbene}$ interatomic distances for **1**-**3** (~2.03 Å; Table 1) show almost no variations because Zn^{II} does not undergo π-back donation, and thus the bonding interaction is purely of σ-type. Indeed, shorter Zn–$C^{carbene}$ were reported only for stronger σ-donating carbenes, such as in [$ZnCl_2$(CDP')] (1.994(2) Å).[12] The angle Ω between the two planes defined by the ZnX_2 atoms and the carbene heterocycle (Figure 2C) slightly increases for the heavier halides (**1**: 69.7º, **2**: 70.3º, **3**: 71.5º). These values are higher in comparison with other trigonal planar zinc(II) halide carbenes mentioned above, e.g., [$ZnCl_2$(CDP')] (65.2º)[12] and [$ZnCl_2$(7-Dipp)] (58.7º),[15] due to the fact that ITr is one of the bulkiest NHC reported so far, enforcing a more close-to-perpendicular orientation of ITr towards the [ZnX_2] plane.

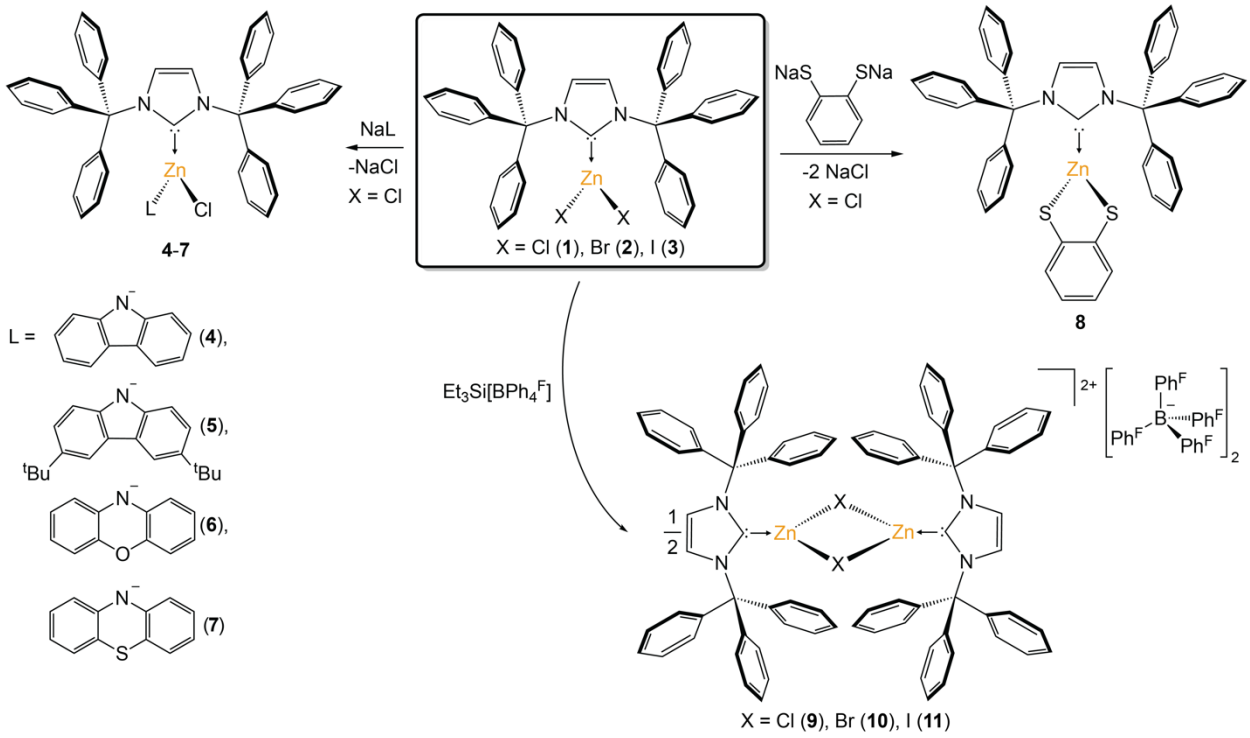

Scheme 1. Reactivity of monomeric ITr complexes **1**-**3**.

Halide exchange and abstraction reactions of 1-3

To explore the chemistry of the low-coordinated Zn^{II} complexes **1**-**3**, we performed a series of reactions focused on halide ligand exchange and abstraction. As shown in Scheme 1, the reaction of the chloride derivative **1** with one equiv. of deprotonated phenoxazine, phenothiazine or carbazoles (CzH) to give complexes of the type [ZnCl(L)(ITr)], where L = carbazolate (**4**), 3,6-di-tert-butylcarbazolate (**5**), phenoxazine (**6**), phenothiazine (**7**). The ^{1}H NMR spectra of complexes **4** and **5** reveal a 1:1 ratio of the resonances of the carbazolate and ITr ligand, which confirms the successful selective exchange of one chloride ligand. Moreover, a singlet at ~7.18 ppm with an integral intensity of 2 is found for the C–*H* protons of the ITr ligand, implying C_s symmetry of the complexes. In contrast, the aromatic hydrogen resonances of the Cz ligands show an asymmetric

pattern, which suggests that these ligands lie in the σ mirror plane, meaning perpendicular orientations towards the plane of the ITr heterocycle. We note that the ^{1}H resonances of the *tert*-butyl substituents in **5** are rather broad, as the phenyl rings of the ITr ligand apparently hinder the free ligand rotation. Very similar behavior was found for the structurally closely related Zn^{II} compounds **6** and **7**. These two complexes appear unstable in solutions as we observed contaminations of the NMR samples with unspecified by-products even though fresh, single-crystalline material was used for the characterization by NMR spectroscopy in the case of **6**. However, complexes **4**-**6** were further characterized by X-ray diffraction analysis using single crystals obtained from a toluene/*n*-pentane mixture at -40 ºC (**4** and **5**) or DCM/*n*-pentane at room temperature (**6**) (Figure 3). In line with the NMR spectroscopic analysis, the amide complexes **4**-**6** adopt a distorted trigonal-planar arrangement around the Zn^{II} ion analogous to the halide complexes **1**-**3**, and the N-donor ligand is oriented perpendicularly to the plane of the ITr heterocycle. The steric demand of the amides leads to a further increase of the Ω angles (~86º) in comparison to **1**-**3** (~70º). The interatomic distances Zn–$C^{carbene}$ of ~2.04 Å are very similar to **1**-**3**; however, as shown in Table 1, the Zn–Cl and Zn–N bond lengths increase slightly in the order: **4** < **5** < **6**.

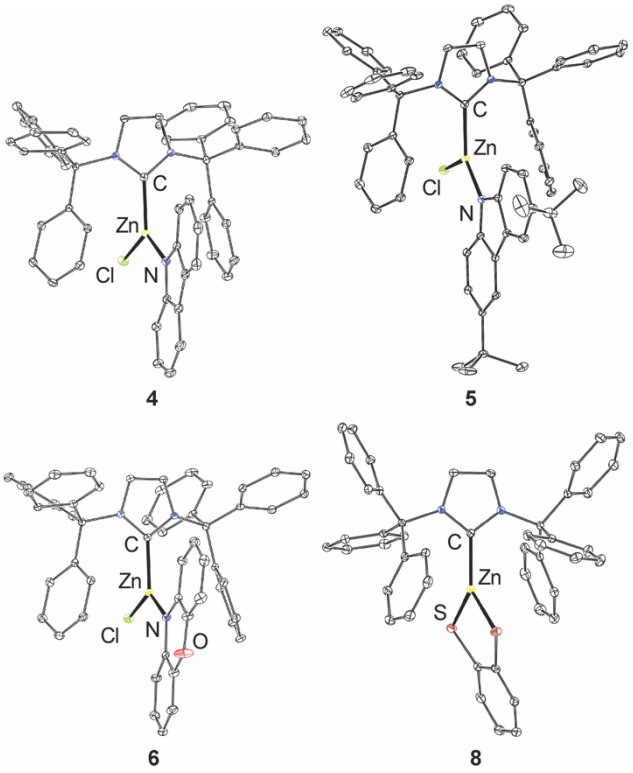

Figure 3. Molecular structures of **4**-**6** and **8**. Thermal ellipsoids are drawn at a 30% probability level, and hydrogen atoms together with co-crystallized molecules of solvents are omitted for clarity. Selected interatomic distances and angles are listed in Table 1.

The reaction of complex **1** with disodium 1,2-benzedithiolate (Na_2bdt) resulted in the exchange of both chloride ligands to give [Zn(bdt)(ITr)] (**8**) (Scheme 1) as confirmed by ^{1}H and ^{13}C NMR spectroscopic measurements, and X-ray diffraction analysis. The chelating coordination and higher rigidity of the bdt ligand led to a more pronounced distortion of the complex geometry than in the case of relatively flexible **1**-**7**. The bdt ligand is bent as demonstrated by the ^{carbene}C–Zn–C_g^{bdt} angle (where C_g^{bdt} is the centroid of the aromatic ring of the bdt ligand) of 164.88(2)º, which is a configuration typical for various thiolate ligands. Furthermore, the bidentate

coordination mode of bdt enforces a small S–Zn–S angle of only 98.38(2)º and a concomitant larger angle S–Zn–$C^{carbene}$ of ~130º.

Table 1. Selected geometrical parameters of ITr complexes **1-11**. For definition of angels α and Ω, see Figure 2C.

	Zn–X [Å]	Zn–E [Å] [a]	Zn–$C^{carbene}$ [Å]	α [º]	Ω [º]
1	2.2170(5) 2.2022(5)	-	2.0322(13)	359.92(3)	69.38(3)
2	2.3559(5) 2.3400(5)	-	2.0322(12)	359.94(3)	69.98(4)
3	2.5391(7) 2.5575(7)	-	2.034(5)	359.96(8)	71.17(3)
4	2.1951(6)	1.9400(16)	2.0335(19)	359.99(6)	86.25(13)
5	2.2129(9)	1.9440(18)	2.0511(17)	360.01(7)	87.47(18)
6	2.2222(7)	1.956(2)	2.047(2)	360.00(8)	87.54(4)
8	-	2.2426(7) 2.2425(7)	2.007(2)	359.65(5)	72.25(15)
9	2.2566(5) 2.3266(7)	-	1.9775(15)	358.14(4)	75.59(8)

	2.5637(6)				
11		-	1.997(4)	358.01(7)	72.47(12)
	2.6659(6)				

[a] E = N (**4**-**6**), S (**8**)

The isolation of even lower-coordinated zinc complexes for reactivity or luminescence studies is very challenging, which motivated us to investigate a potential route for the preparation of two-coordinated Zn^{II} compounds using halide abstraction of **1**-**3**. For the cleavage of the Zn–X bonds, we used a strongly halophilic silylium-like reagent, $[Et_3Si(toluene)][BPh^F_4]$ (Ph^F = pentafluorophenyl), previously successfully employed for chloride abstraction from [AuCl(^{Ad}cAAC)] (^{Ad}cAAC = adamantyl-substituted cyclic(alkyl)(amino)carbene).[22] The abstraction reaction was performed in toluene suspensions of **1**-**3** with one equivalent of in-situ generated halophile (Scheme 1). After evaporation of the volatiles, products were extracted with DCM and crystallized from a DCM/*n*-pentane mixture, yielding pale yellow to yellow single crystals of **9**-**11**. Characterization by multinuclear NMR spectroscopy revealed patterns that resemble those described above for **1**-**3**. Most importantly, the $C^{carbene}$ resonances with chemical shifts ~167 ppm are found for all samples in the low-field area of the ^{13}C spectra. This proves that the ITr carbene remains coordinated after the abstraction reactions. Moreover, these values are ca. 7 ppm upfield shifted compared to the starting complexes **1**-**3**, the shift implying a stronger bond between Zn^{II} and the carbene due to the cleavage of the anionic halide ligands and the formation of a cationic complexes with increased electron deficiency on the metal center. A similar trend was observed for ^{15}N NMR resonances for **9**-**11**, which are more slightly shifted towards high field (~-171 ppm) compared to values recorded for **1**-**3** (~-169 ppm), further proving enhanced ITr →

Zn σ-donation for molecules **9**-**11**.[23] The formation of the cationic species was evidenced by ^{19}F spectra clearly showing resonances corresponding to the $[BPh^{F}_{4}]^{-}$ counter anion. Finally, compounds **9**-**11** were characterized by X-ray diffraction analysis which confirmed the abstraction of one halide; however, dimers of the type $[\{Zn(\mu\text{-}X)(ITr)\}_2][BPh^{F}_{4}]_2$ (X = Cl (**9**), Br (**10**), I (**11**)), instead of two-coordinated monomers were obtained (Scheme 1 and Figure 4). Although for **10** the X-ray diffraction analysis gave low-quality data, which prevents a detailed discussion of structural parameters for this complex, all molecules **9**-**11** feature both a rare trigonal planar coordination mode and cationic nature, uncommon for carbene complexes of zinc. The dimeric complexes crystalize in the $P2_1/n$ space group with one molecule of DCM (**9** and **11**) or *n*-pentane (**10**) co-crystallized in the unit cell. For **9** and **11**, the trigonal planar coordination environment is confirmed by the α angles reaching 360º analogous to **1**-**8**. However, the bridging mode of halides significantly distorts the ideal trigonal planar geometry, as evidenced by X–Zn–X angles of ~90º, and elongates Zn–X bonds compared to the starting monomers (Table 1). The $[Zn_2X_2]$ cluster-like backbones of **9** and **11** are asymmetric and show a significant variation of Zn–X bond distances (up to 0.07 and 0.1 Å for **9** and **11**, respectively) which reflects the bridging coordination mode of halide ligands. In contrast, the $Zn–C^{carbene}$ bonds are shortened, reflecting the electron deficiency on the cationic metal center and enhanced ITr → Zn σ-donation, which is in line with the aforementioned ^{13}C signals of the $C^{carbene}$ and ^{15}N resonances of the ITr ligand. The value (~75º) of the angle Ω is in between those observed for **1**-**3** and **4**-**6**. Compounds **9**-**11** in dichloromethane solutions were further characterized by mass spectrometry (MS) that revealed extensive fragmentation upon ionization of the initial dimeric arrangements to monomeric, monocationic fragments $[Zn(ITr)(X)]^+$ (m/z = 651 (**9**), 697 (**10**), 743 (**11**)). Also, decomposition of the ITr ligand itself is observed with the detection of a cationic Ph_3C^+ fragment (m/z = 243).

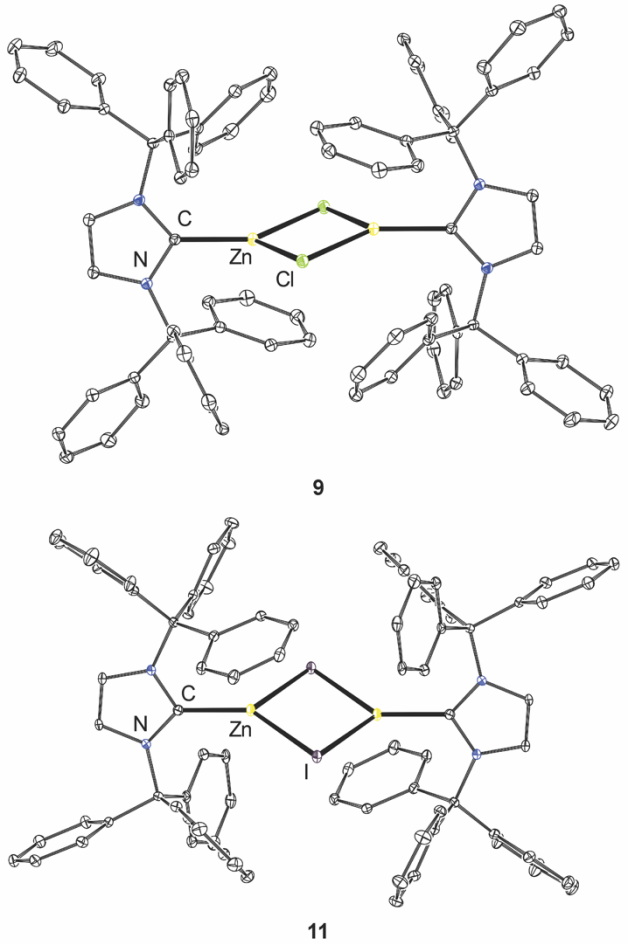

Figure 4. Molecular structures of **9** and **11**. Hydrogen atoms, crystal solvents and counter anions are omitted for clarity. Selected interatomic distances and angles are listed in Table 1.

Photophysical studies

Attempts to obtain complexes **4-7** analytically pure failed, and thus these compounds were excluded from the photophysical study. For **1-3** and **8-11**, the electronic UV/vis absorption spectra in dichloromethane solutions revealed intense, high-energy absorptions below 300 nm likely related to ligand-centered (LC) $\pi\rightarrow\pi^*$ transitions of the ITr fragment. In the case of complex **8**, an additional broad band with λ_{max}^{abs} = 317 nm is observed, which stems from bdt(π)→ITr(π^*_{CN}) LLCT excitations according to our quantum chemical studies (see Figure S31). Interestingly, only **9-11** exhibit low energy absorptions (Figure 5, inset) in the range of 360-480 nm with extinction coefficients ε of 0.3×10^3 (**9**), 2.8×10^3 (**10**) and 3.5×10^3 (**11**) $M^{-1}\cdot cm^{-1}$ that follow the decrease of reduction potential along the series Cl > Br > I. We attribute these bands to halide (p-character lone pair)→ITr(π^*_{CN}) ligand-to-ligand charge transfer (LLCT) excitations, which give rise to two overlapping broad bands with λ_{max} of 410 and 435 nm, respectively, due to the asymmetric bridging bonding mode of the halide ligands (see discussion of crystal structures of **9-11** above).

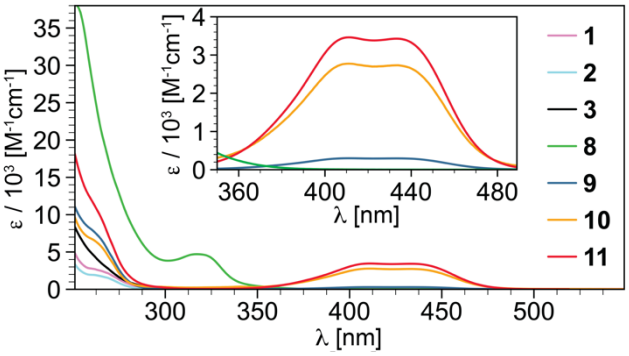

Figure 5. UV/vis absorption spectra of **1-3** and **8-11** in dichloromethane at room temperature.

Although complexes **1**-**3** show broad dual photoluminescence (PL) with λ_{max} = 425 and 570 nm, respectively, upon photoexcitation in the solid state, they are photolabile as we note considerable changes in the luminescence intensity (for details, see ESI). A similar behavior was recently reported for cyclic (alkyl)(amino)carbenes (cAAC) of zinc(II) bearing halide ligands, for which one of the photo-induced decomposition pathways was identified to be an asymmetric distortion upon cAAC rotation.[4] An analogous process could be responsible for the photo-induced transformation of **1**-**3**. In contrast, compounds **8**-**11** are photostable upon irradiation in the solid state because of the enhanced rigidity imposed by the bidentate or bridging ligands. Thus, more detailed photophysical studies were performed using these selected samples.

Table 2. Selected photophysical data for **1-3** and **8-11** in the solid state.

	T [K]	λ_{ex} [nm]	λ_{em}^{max} [nm]	τ [ms] [a]	Φ	k_r [s^{-1}] [b]
8	297	380	554	9.03	0.04	4.4
9	297	400	584	0.080	0.04	500
	77	440	560	135	0.19	1.4
10	297	450	594	0.068	0.02	294
	77	450	560	3.62	0.06	16.7
11	297	450	610	0.014	0.004	286
	77	450	562	79	0.03	0.38

[a] amplitude average lifetime (for details of the multiexponential decay deconvolution, see Table S3), [b] $k_r = \Phi/\tau$

Photoexcitation of **8** into the lowest-energy absorption band results in broad green-to-yellow photoluminescence with λ^{max} = 552 nm (Figure 8A) that can be attributed to a bdt → ITr excitation of LLCT character, analogous to the recently reported dimer [(^{Me}cAAC)Zn(*kS*:μ^2*S*-PhS_2)$_2$Zn(^{Me}cAAC)].[5] Moreover, lifetime measurements revealed exceptionally long-lived excited states with an average lifetime <τ> of 9028 µs, which together with a quantum yield Φ of 0.04 suggests a radiative rate constant k_r = 5 s^{-1}, proving spin-forbidden phosphorescence.

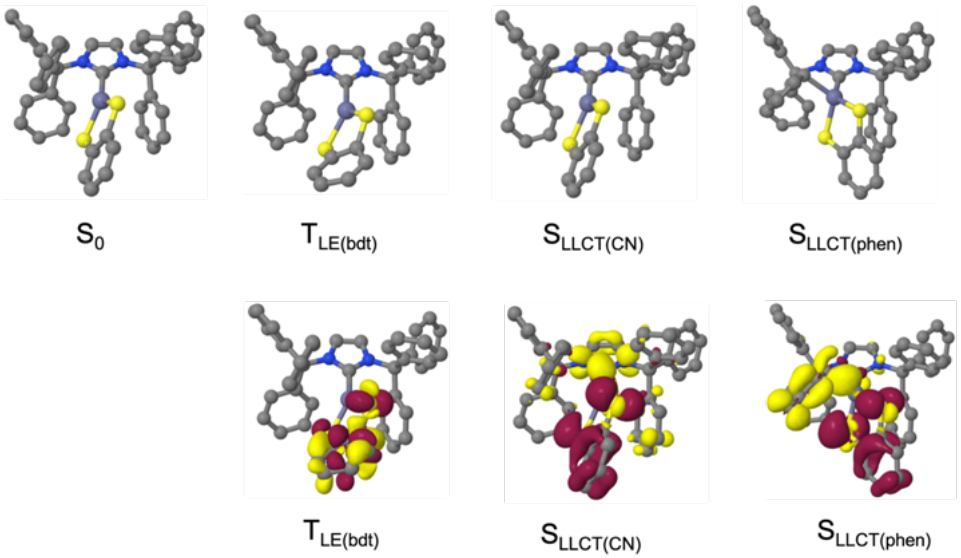

Figure 6. Nuclear arrangements (upper panel) and difference densities (lower panel) of selected electronic states of **8** at their respective minimum geometry in DCM. Hydrogen atoms are not shown. Red areas indicate a loss of electron density in comparison to the electronic ground state, yellow areas a gain. $T_{LLCT(CN)}$ and $T_{LLCT(phen)}$ closely resemble their singlet counterparts and have been omitted.

Our quantum chemical calculations reveal that the $T_{LLCT(CN)}$ state resulting from the bdt(π)→ITr(π^*_{CN}) excitation is not the lowest triplet state of this complex. In the Franck–Condon region, a local triplet excitation on the bdt ligand is practically degenerate with the ^{1}LLCT(CN) S_1 state (Figure S31). Adiabatically, the ^{3}LC(bdt) state forms the global minimum on the T_1 potential energy surface. Upon geometry relaxation, the C_1-C_2 bond of the benzene ring loses its double bond character and elongates to 150 pm. To reduce the steric strain on the chelating centers, the bdt ligand gives up its planarity. Therefore, the ^{3}LC(bdt) emission is broad and structureless, despite its local transition character. The computed phosphorescence rate constant (43 s^{-1}) of the

^{3}LC(bdt) emission is somewhat larger than the measured radiative rate constant of k_r = 5 s^{-1}. The nonradiative deactivation of the ^{1}LLCT(CN) state might be related to somewhat weaker π-electron density accepting properties in the excited states of N-heterocyclic carbenes compared to cAAC,[24] which results in higher LLCT excitation energies for **8** and makes the ^{3}LC(bdt) state accessible. Although a couple of recently published articles reported the population of triplet excited states in the case of Zn^{II} molecules, such a photophysical behavior remains uncommon for the complexes based on light and earth-abundant zinc metal.[2,3,25]

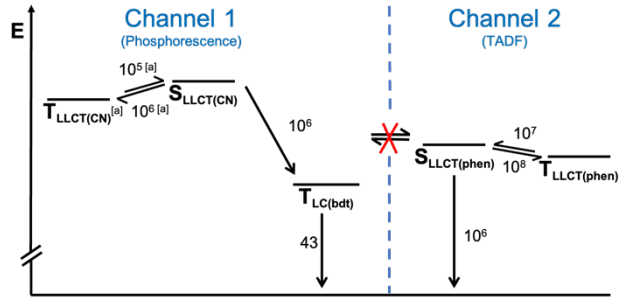

Figure 7. Proposed decay schemes of the LLCT(CN) states (left) and LLCT(phen) states of **8** (right). The LLCT(CN) states originate from a bdt-to-ITr charge transfer involving the antibonding π^*_{CN} orbital of the carbene. They are the lowest excited states in the Franck–Condon region and deactivate readily to the phosphorescent $T_{LC(bdt)}$ state. In the LLCT(phen) states, a covalent bond is formed between a phenyl carbon atom and the zinc center. They are predicted to show TADF but are difficult to access. ISC and rISC rate constants (s^{-1}) were determined for room temperature employing DFT/MRCI energies and wavefunctions at BH-LYP optimized geometries except for the $T_{LLCT(CN)}$ state where a PBE0 optimized geometry had to be used instead. Quantities determined for PBE0 optimized geometries have been marked by [a] in the scheme on the left.

In addition to the above mentioned LLCT states in which the carbene π^*_{CN} orbital is the accepting orbital, the calculations find low-lying singlet and triplet states referred to as LLCT(phen) in the following. They originate from bdt(π)→ITr(π^*_{phen}) excitations populating the π^* orbital of the ITr phenyl residue located closest to the metal center. They lie quite high in energy in the Franck–Condon region but are stabilized by the formation of a covalent C–Zn bond in the excited state where the Zn center is tetragonally coordinated (Figure 6). Adiabatically, the ^{1}LLCT(phen) state forms the lowest excited singlet state. The calculations predict this state to show efficient orange TADF at the sub-microsecond time scale, provided that its minimum can be reached.

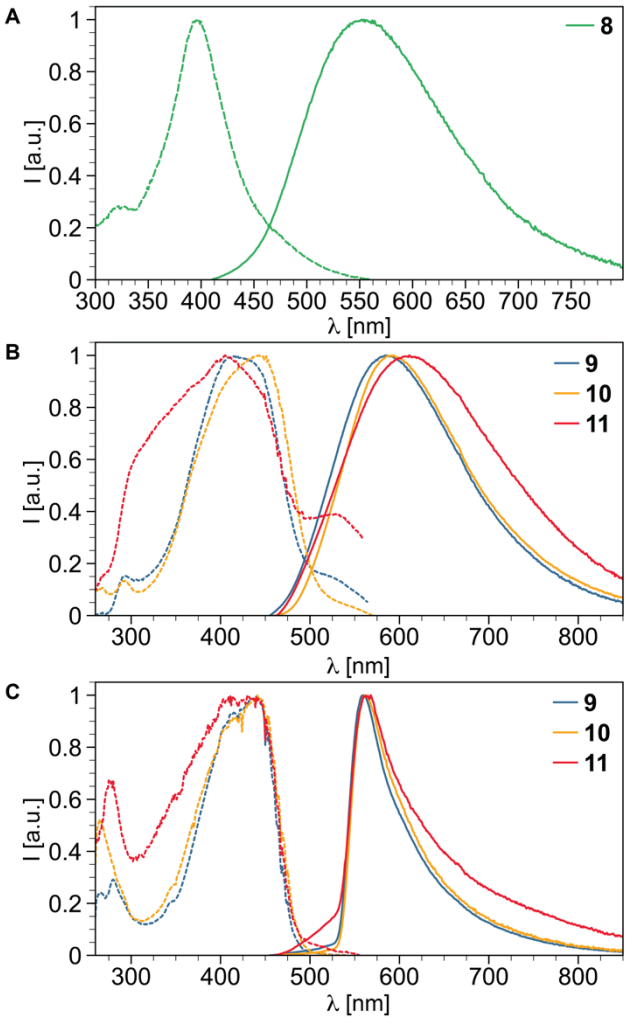

Figure 8. Excitation (dashed) and emission (solid) profiles in the solid state. **A**: **8** at 297 K (λ_{em} = 580 nm, λ_{ex} = 380 nm), **B**: **9-11** at 297 K (λ_{em} = 580-590 nm, λ_{ex} = 450 nm), **C**: **9-11** at 77 K (λ_{em} = 560 nm, λ_{ex} = 450 nm).

Upon photoexcitation between 360-480 nm, the dimers **9-11** show orange PL in the solid state at room temperature associated with considerably broad spectral features (Figure 8B) with full width at half maximum (FWHM) in the range of 4070-5320 cm^{-1}. The emission maxima slightly shift bathochromically in the series **9** (584 nm) < **10** (594 nm) < **11** (610 nm), reflecting a more

pronounced contribution of the heavier halide ligands to the emissive excited states of X → ITr LLCT character. We recorded long PL lifetimes in the range of tens of μs (Tables 2 and S3) and PL quantum yields Φ = 0.02-0.04, giving k_r of 286-500 s^{-1} indicative for phosphorescence. As shown in Figure 8C, the spectral appearance of the emission change considerably upon cooling to 77 K with narrow profiles (FWHM = 1910-2440 cm^{-1}) and hypsochromic shifts of λ^{max} to ca. 562 nm for all samples. In addition, the lifetimes increase by 2-3 orders of magnitude with a concomitant decrease of k_r to the same degree (Table 2). Considering the very similar emission profiles of **9**-**11** at 77 K (Figure 8C), the emissive states at low temperatures appear to involve only minor halide contributions. Also, the λ_{max} are comparable to the phosphorescence of the triphenylmethyl cation (550 nm),[26] which suggests that the luminescent states of **9**-**11** at 77K are localized on the triphenylmethyl groups of the ITr ligand. In contrast, the emissive states at room temperature are likely of LLCT character and apparently require a thermally driven population.

CONCLUSION

We have prepared, isolated and structurally characterized a novel series of Zn^{II}/N-heterocyclic carbene complexes featuring an atypical trigonal coordination mode. A detailed study of the chemical behavior of the halide complexes of the type [ZnX_2(ITr)] (X = Cl (**1**), Br (**2**), I (**3**)) demonstrates a highly flexible coordination sphere. The chloride ligands of **1** can be efficiently exchanged in partial or exhaustive manner to give additional trigonal planar complexes bearing various mono- or di-anionic ligands. In addition, halide abstraction yielded structurally unprecedented, dimeric molecules [{Zn(μ-X)(ITr)}$_2$][BPh^F_4]$_2$ (X = Cl (**9**), Br (**10**), I (**11**)) with cationic character. Photophysical studies, including low-temperature experiments, further show visible light photoluminescence of all new trigonal planar complexes of zinc. Although the starting

molecules **1-3** are photolabile, compounds **8-11** with exchanged/abstracted halide ligands and improved rigidity are photostable. Lifetime measurements revealed long-lived excited states due to the population of triplet excited states. In the case of [Zn(bdt)(ITr)] (**8**), the combined experimental/theoretical survey revealed long-lived phosphorescence (millisecond region) from the ^{3}LC(bdt) excited state. This finding is in stark contrast to carbene-zinc-thiolate emitters based on cyclic(alkyl)(amino)carbenes (cAAC), showing fast TADF.[5] For **8**, the π^* orbital located on carbene lies higher in energy than in the cAAC complexes, destabilising the 1/3LLCT (bdt $\rightarrow$ ITr) states. As a result, ITr-Zn^{II}-thiolate **8** preferably populates ^{3}LC(bdt) electronically excited state, yielding long-lived phosphorescence potentially useful for photocatalytic or photochemical transformations, which we are currently investigating.

EXPERIMENTAL

General remarks. All operations were performed under an argon atmosphere using conventional Schlenk-line or glovebox techniques. The solvents were dried using a Technology Inc. Pure-Solv system or standard methods,[27] degassed, and stored over activated 4Å molecular sieves. ITr·HBF_4 was prepared according to the procedure described in the literature (for details, see ESI).[19–21] Zinc halides were dried by heating (up to 100 °C) under a high vacuum. All other starting materials were available commercially and were used without further purification. ^{1}H, $^{13}C\{^{1}H\}$ APT, ^{1}H-^{13}C HSQC, ^{1}H-^{13}C HSMB, ^{1}H-^{1}H COSY and ^{1}H-^{15}N HMBC were measured at 300 K on Bruker 500 Avance and Bruker 600 Avance spectrometers. The chemical shifts are given in ppm relative to residual signals of the solvent [^{1}H, ^{13}C: THF-d_8 (1.72, 25.31 ppm), benzene-d_6 (7.16, 128.06 ppm), DCM-d_2 (5.32, 53.84 ppm)]. MALDI-HRMS spectra of the samples in DCTB matrix were recorded on a Thermo Scientific Q Exactive in positive ion mode connected with a TransMIT AP-SMALDI containing a laser with a wavelength of 343 nm and an attenuator of 38° or 40°.

Photophysical Measurements. All photophysical measurements were performed in dry and de-aerated solutions or single-crystalline form. UV/vis absorption spectroscopy was performed using an Agilent Cary 5000 spectrophotometer using standard 1 cm path length quartz cells. Excitation and emission spectra were recorded on an Edinburgh Instrument FLS1000 spectrometer, equipped with a 450 W Xenon arc lamp, double monochromators for the excitation and emission pathways, and a red-sensitive photomultiplier (PMT-980) as a detector. The excitation and emission spectra were corrected using the standard correction files supplied by the manufacturer for the excitation source's spectral power and the detector's sensitivity. Quantum yields in the solid state were measured using an FLS1000 spectrometer equipped with an integrating cryosphere (Microstat N2)

from Oxford Instruments. The luminescence lifetimes were measured using a μF2 pulsed 60 W Xenon microsecond flashlamp, with a repetition rate of 100 Hz and a multichannel scaling (MCS) module or with VPLEDs (449.6 nm with 37 mW), with 100 ns pulse width and an MCS module, dependent on the time range. The emission was collected at a 90° angle to the excitation source. The low-temperature experiments were performed using a liquid nitrogen-cooled OptistatDN-V cryostat from Oxford Instruments.

X-ray diffraction. The crystals of **1–6**, **8**, **9** and **11** were immersed in a film of NVH or perfluoropolyether oil, mounted on a polyimide microloop (MiTeGen) and transferred to a stream of cold nitrogen (Bruker Kryoflex2), and measured at a temperature of 100 K. The X-ray diffraction data were collected on a Bruker D8 diffractometer with a CMOS Photon 100 and multilayer optics monochromated MoKα (0.71073Å) radiation (INCOATEC microfocus sealed tube). The frames were integrated with the Bruker SAINT software package using a narrow-frame algorithm. The APEX3 v2018.7-0 program package was used for cell refinements and data reductions. The structure was solved using the intrinsic phasing method,[28] refined and visualized with the OLEX2-1.5 program.[29] A semiempirical absorption correction (SADABS) was applied to all data. All non-hydrogen atoms were refined anisotropically. Hydrogen atoms were included in structure factors calculations. All Hydrogen atoms were assigned to idealized geometric positions. The unit cells of **4**, **5**, **9**, and **11** contain disordered solvent molecules, which have been treated as a diffuse contribution to the overall scattering without specific atom positions by SQUEEZE/PLATON.[30] The crystallographic details are summarized in Tables S1 and S2. CCDC **2234337**–**2234345** contain the supplementary crystallographic data for this paper.

Quantum chemical methods. The calculations follow a similar computational protocol as previous theoretical studies on other Zn(carbene)(bdt) complexes.[31] In short, the Gaussian 16

program package[32] was utilized for performing all geometry optimizations and vibrational frequency analyses. The def-SV(P) basis set was utilized for first- and second-row atoms.[33] For a better representation of the thiolate charges, the sulfur basis set was augmented by a diffuse s, p, and d function.[34] For Zn, a relativistic effective core potential and the associated contracted 6s5p3d basis set were chosen.[35] In order to account for electrostatic solvent-solute interactions, the PCM model[36] was employed. The equilibrium geometry of the electronic ground state was determined using Kohn-Sham density functional theory (DFT) with the BH-LYP functional[37] and Grimme D3 dispersion corrections[38]. For the singlet excited-state geometries, time-dependent density functional (TDDFT) calculations were performed while the Tamm-Dancoff approximation was used for the triplet geometries. In one case, the PBE0 functional[39] had to be used in this step because a minimum could not be located when the BH-LYP functional was employed. Excitation energies and electric dipole transition moments were calculated using the DFT/MRCI method employing the R2018 Hamiltonian (short parameter set, energy selection threshold Esel=0.8 E_h, 21 singlet and 20 triplet roots).[40] Spin–orbit coupling matrix elements and multiplicity-mixed wavefunctions required to determine probabilities of spin-forbidden transitions were calculated with SPOCK.[41] Rate constants for forward and reverse ISC were obtained within the Franck–Condon (FC) approximation using the VIBES program.[42] The integration of the autocorrelation function was performed on a time interval of 3000 fs using 65536 grid points and a Gaussian damping function of 10 cm^{-1} width.

Synthesis

[$ZnCl_2$(ITr)] (**1**)

300 mg (0.47 mmol) of ITr·HBF_4 and 90 mg (0.49 mmol) of NaHMDS were balanced to a Schlenk tube, 30 mL of toluene was added using a cannula, and the mixture were stirred at room temperature overnight. After that, the suspension was filtrated, and solvents were vacuum evaporated to dryness. The solid residue was mixed with 50 mg (0.37 mmol) of $ZnCl_2$, and 15 mL of THF was added. The obtained clear solution was stirred for two hours at room temperature in the dark and then layered with 15 mL of toluene. After complete diffusion of solvents (~2 days), the formed single-crystals were isolated and washed with toluene (1 × 7 mL), n-pentane (3 × 5 mL) and vacuum-dried for 6 hours at 50 ºC. Yield: 163 mg (0.24 mmol, 65 %). ^{1}H NMR (400 MHz, THF-d_8, 25°C): δ [ppm] =7.38-7.31 (m, 23H, C(C_6H_5)$_3$), 7.27-7.24 (m, 7H, C(C_6H_5)$_3$), 7.18 (s, 2H, C*H*). ^{13}C NMR (150 MHz, THF-d_8, 25°C): δ [ppm] = 176.1 (s), 143.0 (s), 138.4 (s, *toluene*) 131.6 (s), 130.6 (s), 130.5 (s), 130.4 (s), 130.2 (s), 129.7 (s, *toluene*) 129.1 (s, *toluene*), 128.9 (s), 128.6 (s), 128.4 (s), 127.8 (s), 127.6 (s), 126.0 (s, *toluene*), 125.1 (s), 80.0 (s), 21.5 (s, *toluene*). ^{15}N-NMR (60 MHz, THF-d_8, 25°C): δ [ppm] = -169.7. CHNS analysis calcd for $C_{48}H_{40}N_2ZnCl_2$ (C_7H_8): C, 73.80; H, 5.16; N, 3.59. Found: C, 72.9; H, 5.2; N, 3.9.

[$ZnBr_2$(ITr)] (**2**)

Complex **2** was prepared using the same procedure as described for **1** but with 510 mg (0.79 mmol), 90 mg NaHMDS (0.83 mmol) and 143 mg of $ZnBr_2$ (0.64 mmol). Yield: 359 mg (0.46 mmol, 58 %) of pale-yellow needle-like crystals. ^{1}H NMR (400 MHz, THF-d_8, 25°C): δ [ppm] =7.37-7.32 (m, 23H, C(C_6H_5)$_3$), 7.28-7.25 (m, 7H, C(C_6H_5)$_3$), 7.17 (s, 2H, C*H*). ^{13}C NMR (125

MHz, THF-d_8, 25°C): δ [ppm] = 175.4 (s), 142.9 (s), 130.5 (s), 130.4 (s), 129.6 (s), 129.0 (s), 128.9 (s), 126.0 (s), 125.3 (s), 80.2 (s). ^{15}N NMR (50 MHz, THF-d_8, 25°C): δ [ppm] = -170.3. CHNS analysis calcd for $C_{48}H_{40}N_2ZnBr_2\cdot(C_7H_8)$: C, 66.26; H, 4.63; N, 3.22. Found: C, 66.6; H, 4.8; N, 3.5.

[ZnI_2(ITr)] (**3**)

Complex **3** was prepared using the same procedure as described for **1** but with 500 mg of ITr·HBF_4 (0.78 mmol), 90 mg NaHMDS (0.83 mmol) and 199 mg of ZnI_2 (0.62 mmol). Yield: 166 mg (0.19 mmol, 24 %) of pale-yellow needle-like crystals. ^{1}H NMR (600 MHz, THF-d_8, 25°C): δ [ppm] =7.36-7.35 (m, 24H, C(C_6H_5)$_3$), 7.30-7.26 (m, 6H, C(C_6H_5)$_3$), 7.15 (s, 2H, C*H*). ^{13}C NMR (150 MHz, THF-d_8, 25°C): δ [ppm] = 173.8 (s), 142.9 (s),138.4 (s), 130.8 (s), 130.6 (s), 129.7 (s), 129.2 (s), 128.9 (s), 126.0 (s), 125.5 (s), 80.6 (s).^{15}N NMR (60 MHz, THF-d_8, 25°C): δ [ppm] = -170.1. CHNS analysis calcd for $C_{48}H_{40}N_2ZnI_2\cdot(C_7H_8)$: C, 59.80; H, 4.18; N, 2.91. Found: C, 59.6; H, 4.2; N, 3.0.

[ZnCl(Cz)(ITr)] (**4**)

To a solution of complex **1** (50 mg, 64 μmol) in 3 mL of THF was slowly added a solution of 13 mg (70 μmol) sodium carbazolate (NaCz) in 3 mL of THF. The reaction mixture was stirred overnight at room temperature. After that, the solvents were vacuum-evaporated, and the solid residue was extracted with toluene (3 × 5 mL). The toluene solution was concentrated by vacuum evaporation, mixed with *n*-pentane and stored at -40ºC for two days. During this time, white single-crystals were formed. The supernatant was discarded, and crystals were washed with 5 mL of *n*-

pentane and vacuum-dried. Yield: 30 mg (36 µmol, 56 %). ^{1}H NMR (500 MHz, THF-d_8, 25°C): δ [ppm] = 7.91-7.86 (m, 2H), 7.60-7.59 (m, 1H), 7.33-7.32 (m, 11H), 7.26-7.23 (m, 2H), 7.19 (s, 2H), 7.13-7.02 (m; 19H), 6.89-6.85 (m; 2H). ^{13}C NMR (125 MHz, THF-d_8, 25°C): δ [ppm] = 176.4 (s), 142.3 (s), 130.7 (s), 129.8 (s), 129.6 (s), 129.1 (s), 128.9 (s), 126.9 (s), 126.0 (s), 80.7 (s). ^{15}N NMR (50 MHz, THF-d_8): δ [ppm] = -170.5.

[ZnCl(^{tBu}Cz)(ITr)] (**5**)

Complex **5** was prepared using the same procedure as for **4** but with 40 mg (123 µmol) of sodium 3,6-di-*tert*-butyl-carbazolate (Na^{tBu}Cz). Yield: 54 mg (58 µmol, 49 %). ^{1}H NMR (600 MHz, benzene-d_6, 25°C): δ [ppm] = 8.53 (d, $^{2}J_{H-H}$= 31.7 Hz, 2H), 8.20 (d, $^{3}J_{H-H}$= 7.6 Hz 1H), 7.63 (dd, , $^{3}J_{H-H}$= 7.5 Hz, $^{2}J_{H-H}$= 56.3 Hz, 2H), 7.39-7.38 (m, 12H), 7.18 (d, $^{3}J_{H-H}$= 8.6 Hz, 1H) 6.92-6.90 (m, 12H), 7.02-6.99 (m; 5H), 6.80-6.78 (m; 6H), 6.56 (s, 1H), 1.60 (d; , $^{3}J_{H-H}$= 24.2 Hz, 18H). ^{13}C NMR (150 MHz, benzene-d_6, 25°C): δ [ppm] = 177.2 (s), 141.5 (s), 130.1 (s), 129.4 (s), 128.8 (s), 128.3 (s), 125.4 (s), 122.8 (s), 120.7 (s),116.5 (s), 116.0 (s), 115.1 (s), 112.7 (s), 80.4 (s), 34.8(s), 32.7 (d, J_{C-C}= 8.4 Hz). ^{15}N NMR (60 MHz, benzene-d_6): δ [ppm] = -171.46.

[ZnCl(ITr)(pnz)] (**6**)

To a solution of complex **1** (50 mg, 73 µmol) in 5 mL of THF, 15 mg (73 µmol) of sodium phenoxazine was added. The reaction mixture was stirred overnight at room temperature. After that, the mixture was filtered through celite, and solvents were vacuum-evaporated. The solid residue was extracted with 7 of mL toluene. Gas phase diffusion of *n*-pentane into the toluene solution afforded yellow-green single crystals suitable for X-ray diffraction analysis. Yield: 11 mg

(13 μmol, 18 %). The NMR measurement revealed the formation of multiple sets of unidentified signals, implying instability, which prevented the characterization of **6** in solutions.

[ZnCl(ITr)(ptz)] (**7**)

To a solution of complex **1** (30 mg, 44 μmol) in 5 mL of THF was added 13 mg (44 μmol) of sodium phenothiazine. The reaction mixture was stirred overnight at room temperature and filtered through celite. After that, the solvents were vacuum-evaporated, and the solid residue was extracted with 7 mL of toluene. Gas phase diffusion of *n*-pentane into the toluene solution afforded yellow-green crystals of **7**. Yield: 5 mg (5.6 μmol, 14 %). The NMR measurement revealed multiple sets of signals, implying instability of **7** in solutions. ^{1}H NMR (400 MHz, THF-d_8, 25°C, the main set of signals): δ [ppm] = 7.91-7.88 (m, 1H), 7.82-7.77 (m, 1H), 7.37-7.35 (m, 7H), 7.26-7.10 (m, 26H), 6.94-6.82 (m, 2H), 6.77-6.52 (m; 4H).

[Zn(bdt)(ITr)] (**8**)

To a solution of complex **1** (60 mg, 88 μmol) in 3 mL of THF, a solution of 18 mg (96 μmol) sodium benzene-1,2-dithiolate (Na_2bdt) in 3 mL of THF was slowly added. The reaction mixture was stirred overnight at room temperature. After that, the solvent was evaporated to dryness. The solid residue was extracted with 4 mL of DCM, and gas phase diffusion of n-pentane afforded white single crystals. The obtained crystals were collected, washed with toluene (1 × 3 mL) and n-pentane (2 × 3 mL) and vacuum-dried. Yield: 21 mg (29 μmol, 32%). ^{1}H NMR (500 MHz, DCM-d_2, 25°C): d [ppm] =7.37-7.30 (m, 19H), 7.23 (s, 2H), 7.16-7.14 (m, 11H), 6.98-6.96 (m, 2H), 6.46-6.45 (m, 2H). ^{13}C NMR (125 MHz, DCM-d_2, 25°C): d [ppm] = 180.2 (s), 144.8 (s), 141.1 (s), 130.8 (s), 130.0 (s), 129.8 (s), 129.4 (s), 129.2 (s), 128.8 (s), 122.0 (s), 120.8 (s), 79.2 (s). 15N

NMR (50 MHz, DCM-d2): d [ppm] = -169.1. CHNS analysis calcd for $C_{47}H_{36}N_2ZnS_2 \cdot (CH_2Cl_2)_{0.12}$: C, 73.56; H, 4.80; N, 3.62. Found: C, 73.45; H, 4.75; N, 3.7. Even after prolonged drying under a high vacuum, the elemental analysis and ^{1}H NMR spectrum (Figure S12) revealed residual DCM (~12 %) in the sample. Thus, solvent-free single crystals were prepared from the THF/n-pentane mixture for the photophysical measurement.

$[\{Zn(\mu\text{-}Cl)(ITr)\}_2][BPh^F_4]_2$ (**9**)

A solution of 107 mg $Ph_3CBPh^F_4$ (120 µmol) and 0.2 mL of triethylsilane (17 mmol) in 7 mL of toluene was stirred for 30 min at room temperature. The colorless solution was evaporated to dryness, and 80 mg (120 µmol) of complex **1** was added as the solid. 5 mL of toluene was added to the mixture, and the suspension was stirred at room temperature overnight. After that, the solvent was vacuum-evaporated, the solid residue was washed with pentane (2 × 5 mL) and extracted with 6 mL of dichloromethane. The solution was filtrated through celite, and the solution was layered with 6 mL of *n*-pentane. During the diffusion of the anti-solvent, yellow single-crystals of **9** were formed. Yield: 45 mg (17 µmol, 29 %). ^{1}H NMR (400 MHz, THF-d_8, 25°C): δ [ppm] = 7.54 (s, 4H), 7.47-7.42 (m, 36H), 7.27-7.26 (m, 24H). ^{13}C NMR (150 MHz, THF-d_8, 25°C): δ [ppm] = 168.1 (s), 150.0 (s), 148.4 (s), 137.9 (s), 136.3 (s), 130.8 (s), 130.5 (d, $J_{C\text{-}F}$= 9.5 Hz), 130.3 (s), 130.2 (s), 129.0 (s), 128.1 (s), 126.6 (s), 80.4 (s). ^{15}N NMR (60 MHz, THF-d_8): δ [ppm] = -167.7. ^{19}F NMR (60 MHz, THF-d_8, 25°C): δ [ppm] = -132.73 (d, $J_{F\text{-}C}$= 9.5 Hz), -165.10 (t, $J_{F\text{-}F}$= 20 Hz), -168.56 (t, $J_{F\text{-}F}$= 20 Hz). CHNS analysis calcd for $C_{130}H_{64}N_4Zn_2Cl_2B_2F_{40} \cdot CH_2Cl_2$: C, 57.50; H, 2.54; N, 2.02. Found: C, 57.3; H, 2.9; N, 2.1. MALDI-HRMS m/z: 651.1 $[M-C_{41}H_{32}N_2ClZn]^+$, 243.1 $[M-C_{63}H_{51}N_4Cl_2Zn]^+$.

[{Zn(μ-Br)(ITr)}$_2$][BPh$^F_4$]$_2$ (**10**)

Complex **10** was prepared using the same procedure as described for **9** but with 90 mg (120 μmol) of **2**. Yield: 50 mg (17 μmol, 14 %). ^{1}H NMR (500 MHz, THF-d$_8$, 25°C): δ [ppm] = 7.50 (s; 4H), 7.47-7.40 (m, 36H), 7.27-7.25 (m, 24H). ^{13}C NMR (125 MHz, THF-d$_8$, 25°C): δ [ppm] =179.4 (s), 141.9 (s), 130.6(d, $J_{F\text{-}C}$= 6 Hz), 130.2 (s), 126.6 (s), 80.4 (s). ^{15}N NMR (50 MHz, THF-d$_8$): δ [ppm] = -167.9. ^{19}F NMR (470 MHz, THF-d$_8$, 25°C): δ [ppm] = -132.72 (d, $J_{F\text{-}C}$= 10 Hz), -165.10 (t, $J_{F\text{-}F}$= 23 Hz), -168.56 (t, $J_{F\text{-}F}$= 20 Hz). $C_{130}H_{64}N_4Zn_2I_2B_2F_{40}\cdot C_5H_{12}$: C, 57.37; H, 2.71; N, 1.98. Found: C, 57.1; H, 2.9; N, 1.9. MALDI-HRMS m/z: 697.1 [M−$C_{41}H_{32}N_2BrZn$]$^+$, 243.1 [M−$C_{63}H_{51}N_4Br_2Zn$]$^+$.

[{Zn(μ-I)(ITr)}$_2$][BPh$^F_4$]$_2$ (**11**)

Complex **11** was prepared using the same procedure as described for **9** but with 101 mg (120 μmol) of **3**. Yield: 40 mg (14 μmol, 25 %). ^{1}H NMR (400 MHz, THF-d$_8$, 25°C): δ [ppm] = 7.48 (s, 4H), 7.47-7.43 (m, 36H), 7.28-7.26 (m, 24H). ^{13}C NMR (150 MHz, THF-d$_8$, 25°C): δ [ppm] = 168.7 (s), 150.0 (s), 148.4 (s), 142.0 (s), 137.9 (s), 136.3 (s), 130.4 (d, $J_{F\text{-}C}$= 7 Hz), 129.0 (s), 128.1 (s), 126.9 (s), 80.7 (s). ^{15}N NMR (60 MHz, THF-d$_8$): δ [ppm] = -167.4. ^{19}F NMR (60 MHz, THF-d$_8$, 25°C): δ [ppm] = -132.7 (d, $J_{F\text{-}C}$= 10 Hz), -165.1 (t, $J_{F\text{-}F}$= 20 Hz), -168.5 (t, $J_{F\text{-}F}$= 20 Hz). $C_{130}H_{64}N_4Zn_2I_2B_2F_{40}\cdot CH_2Cl_2$: C, 53.95; H, 2.38; N, 1.89. Found: C, 54.1; H, 2.6; N, 1.9. MALDI-HRMS m/z: 743.1 [M−$C_{41}H_{32}N_2IZn$]$^+$, 243.1 [M−$C_{63}H_{51}N_4I_2Zn$]$^+$.

Acknowledgments

This work was supported by Deutsche Forschungsgemeinschaft [DFG, Priority Program SPP 2102 “Light-controlled reactivity of metal complexes” (MA 1051/18-1 and STE 1834/7-1)]. A.B. is grateful to Alexander von Humboldt Foundation for a Research Fellowship grant for Postdoctoral Research. We are also grateful to the DFG for funding of major research equipment (INST 212/430-1 FUGG and INST 212/455-1 FUGG). NMR measurements were funded by the Deutsche Forschungsgemeinschaft (DFG, German Research Foundation) – AVANCE NEO 500: 452669591 and AVANCE NEO 600: 452669688.

References

[1] S. Dagorne, *Synthesis* **2018**, *50*, 3662.
[2] J. A. Kübler, B. Pfund, O. S. Wenger, *JACS Au* **2022**, *2*, 2367.
[3] I. B. Lozada, J. D. Braun, J. A. G. Williams, D. E. Herbert, *Inorg. Chem.* **2022**, *61*, 17568.
[4] O. Mrózek, M. Gernert, A. Belyaev, M. Mitra, L. Janiak, C. M. Marian, A. Steffen, *Chem. Eur. J.* **2022**, *28*, e202201114.
[5] O. Mrózek, M. Mitra, B. Hupp, A. Belyaev, N. Lüdtke, D. Wagner, C. Wang, O. Wenger, C. M. Marian, A. Steffen, *Chem. Eur. J.* **2023**, *29*, e202203980.
[6] A. F. Holleman, N. Wiberg, *Lehrbuch der anorganischen Chemie*, de Gruyter, Berlin, **2007**.
[7] I. Resa, E. Carmona, E. Gutierrez-Puebla, A. Monge, *Science* **2004**, *305*, 1136.
[8] a) J. K. McCusker, *Science* **2019**, *363*, 484; b) A. Steffen, B. Hupp Design of Efficient Emissive Materials in *Comprehensive Coordination Chemistry III,* 3rd ed.; E. Constable, G. Parkin, L. Que Jr, Elsevier, **2021**, pp. 466–502.
[9] D. J. Darensbourg, S. A. Niezgoda, J. D. Draper, J. H. Reibenspies, *Inorg. Chem.* **1999**, *38*, 1356.
[10] E. S. Gruff, S. A. Koch, *J. Am. Chem. Soc.* **1989**, *111*, 8762.
[11] D. Wang, K. Wurst, M. R. Buchmeiser, *J. Organomet. Chem.* **2004**, *689*, 2123.
[12] A. Kroll, H. Steinert, L. T. Scharf, T. Scherpf, B. Mallick, V. H. Gessner, *Chem. Commun.* **2020**, *56*, 8051.
[13] a) N. M. Rajendran, N. Gautam, P. Sarkar, J. Ahmed, A. Das, S. Das, S. K. Pati, S. K. Mandal, *Chem. Commun.* **2021**, *57*, 5282; b) C. Fliedel, S. Mameri, S. Dagorne, T. Avilés, *Appl. Organomet. Chem.* **2014**, *28*, 504.
[14] M. Ma, A. Sidiropoulos, L. Ralte, A. Stasch, C. Jones, *Chem. Commun.* **2013**, *49*, 48.
[15] Richard J. Procter, Marina Uzelac, Jessica Cid, Philip J. Rushworth, and Michael J. Ingleson, *ACS Catal.* **2019**, *9*, 5760.
[16] a) S. Mondal, T. Singh, S. Baguli, S. Ghosh, D. Mukherjee, *Chem. Eur. J.* **2023**, e202300508; b) K. Gour, G. Kundu, S. Dash, K. Vanka, S. Tothadi, S. S. Sen, *Eur. J. Inorg. Chem.* **2023**, e202300167.
[17] a) A. J. Arduengo, H. Dias, F. Davidson, R. L. Harlow, *J. Organomet. Chem.* **1993**, *462*, 13; b) D. Specklin, F. Hild, C. Fliedel, C. Gourlaouen, L. F. Veiros, S. Dagorne, *Chem. Eur. J.* **2017**, *23*, 15908; c) D. Specklin, C. Fliedel, C. Gourlaouen, J.-C. Bruyere, T. Avilés, C. Boudon, L. Ruhlmann, S. Dagorne, *Chem. Eur. J.* **2017**, *23*, 5509; d) G. Schnee, C. Fliedel, T. Avilés, S. Dagorne, *Eur. J. Inorg. Chem.* **2013**, *2013*, 3699.
[18] a) R. Hamze, J. L. Peltier, D. Sylvinson, M. Jung, J. Cardenas, R. Haiges, M. Soleilhavoup, R. Jazzar, P. I. Djurovich, G. Bertrand et al., *Science* **2019**, *363*, 601; b) A. M. T. Muthig, O. Mrózek, T. Ferschke, M. Rödel, B. Ewald, J. Kuhnt, C. Lenczyk, J. Pflaum, A. Steffen, *J. Am. Chem. Soc.* **2023**, *145*, 4438; c) A. M. T. Muthig, M. Krumrein, J. Wieland, M. Gernert, F. Kerner, J. Pflaum, A. Steffen, *Inorg. Chem.* **2022**, *61*, 14833; d) M. Gernert, L. Balles-Wolf, F. Kerner, U. Müller, A. Schmiedel, M. Holzapfel, C. M. Marian, J. Pflaum, C. Lambert, A. Steffen, *J. Am. Chem. Soc.* **2020**, *142*, 8897; e) J. Nitsch, F. Lacemon, A. Lorbach, A. Eichhorn, F. Cisnetti, A. Steffen, *Chem. Commun.* **2016**, *52*, 2932; f) A. M. T. Muthig, J. Wieland, C. Lenczyk, S. Koop, J. Tessarolo, G. H. Clever, B. Hupp, A. Steffen, *Chem. Eur. J.* **2023**, e202300946.
[19] M. M. D. Roy, P. A. Lummis, M. J. Ferguson, R. McDonald, E. Rivard, *Chem. Eur. J.* **2017**, *23*, 11249.

[20] M. M. D. Roy, M. J. Ferguson, R. McDonald, E. Rivard, *Chem. Commun.* **2018**, *54*, 483.
[21] T. Hölzel, A. Belyaev, M. Terzi, L. Stenzel, M. Gernert, C. M. Marian, A. Steffen, C. Ganter, *Inorg. Chem.* **2021**, *60*, 18529.
[22] a) J. B. Lambert, S. Zhang, S. M. Ciro, *Organometallics* **1994**, *13*, 2430; b) J. B. Lambert, S. Zhang, C. L. Stern, J. C. Huffman, *Science* **1993**, *260*, 1917; c) V. Lavallo, G. D. Frey, S. Kousar, B. Donnadieu, G. Bertrand, *PNAS* **2007**, *104*, 13569.
[23] K. C. Mondal, S. Roy, B. Maity, D. Koley, H. W. Roesky, *Inorg. Chem.* **2016**, *55*, 163.
[24] M. Gernert, U. Müller, M. Haehnel, J. Pflaum, A. Steffen, *Chem. Eur. J.* **2017**, *23*, 2206.
[25] a) V. Ferraro, F. Baggio, J. Castro, M. Bortoluzzi, *Eur. J. Inorg. Chem.* **2022**, *e202200119*, e202200119; b) N. Lüdtke, J. Kuhnt, T. Heil, A. Steffen, C. M. Marian, *ChemPhotoChem* **2022**, *e202200142*; c) B. Goswami, T. J. Feuerstein, R. Yadav, S. Lebedkin, P. J. Boden, S. T. Steiger, G. Niedner-Schatteburg, M. Gerhards, M. M. Kappes, P. W. Roesky, *Chem. Eur. J.* **2021**, *27*, 15109; d) Ke Zhang, Xianwen Meng, and Lei He, *Inorg. Chem.* **2023**, *https://doi.org/10.1021/acs.inorgchem.2c03804*.
[26] T. Nishiuchi, H. Sotome, R. Fukuuchi, K. Kamada, H. Miyasaka, T. Kubo, *Aggregate* **2021**, *2*.
[27] W. L. F. Armarego, C. L. L. Chai, *Purification of Laboratory Chemicals*, Elsevier Science & Technology, Jordan Hill, **2009**.
[28] a) G. M. Sheldrick, *Acta Crystallogr. C* **2015**, *71*, 3; b) G. M. Sheldrick, *Acta Crystallogr. A* **2015**, *71*, 3.
[29] O. V. Dolomanov, L. J. Bourhis, R. J. Gildea, J. A. K. Howard, H. Puschmann, *J. Appl. Crystallogr.* **2009**, *42*, 339.
[30] A. L. Spek, *Acta Crystallogr. C* **2015**, *71*, 9.
[31] N. Lüdtke, A. Steffen, C. M. Marian, *Inorg. Chem.* **2022**, *61*, 20896.
[32] Gaussian 16, Revision A.03, M. J. Frisch, G. W. Trucks, H. B. Schlegel, G. E. Scuseria, M. A. Robb, J. R. Cheeseman, G. Scalmani, V. Barone, G. A. Petersson, H. Nakatsuji et al., **2016**; Gaussian Inc. Wallingford CT.
[33] A. Schäfer, H. Horn, R. Ahlrichs, *J. Chem. Phys.* **1992**, *97*, 2571.
[34] D. Rappoport, F. Furche, *J. Chem. Phys.* **2010**, *133*, 134105.
[35] D. Figgen, G. Rauhut, M. Dolg, H. Stoll, *Chem. Phys.* **2005**, *311*, 227.
[36] a) E. Cancès, B. Mennucci, J. Tomasi, *J. Chem. Phys.* **1997**, *107*, 3032; b) B. Mennucci, E. Cancès, J. Tomasi, *J. Phys. Chem. B* **1997**, *101*, 10506.
[37] a) C. Lee, W. Yang, R. G. Parr, *Phys. Rev. B* **1988**, *37*, 785; b) A. D. Becke, *J. Chem. Phys.* **1993**, *98*, 1372.
[38] S. Grimme, J. Antony, S. Ehrlich, H. Krieg, *J. Chem. Phys.* **2010**, *132*, 154104.
[39] a) J. P. Perdew, K. Burke, M. Ernzerhof, *Phys. Rev. Lett.* **1996**, *77*, 3865; b) C. Adamo, V. Barone, *J. Chem. Phys.* **1999**, *110*, 6158.
[40] a) S. Grimme, M. Waletzke, *J. Chem. Phys.* **1999**, *111*, 5645; b) C. M. Marian, A. Heil, M. Kleinschmidt, *WIREs Comput. Mol. Sci.* **2019**, *9*, e1394; c) A. Heil, M. Kleinschmidt, C. M. Marian, *J. Chem. Phys.* **2018**, *149*, 164106.
[41] a) M. Kleinschmidt, C. M. Marian, *Chem. Phys.* **2005**, *311*, 71; b) M. Kleinschmidt, J. Tatchen, C. M. Marian, *J. Chem. Phys.* **2006**, *124*, 124101.
[42] a) M. Etinski, J. Tatchen, C. M. Marian, *J. Chem. Phys.* **2011**, *134*, 154105; b) M. Etinski, J. Tatchen, C. M. Marian, *Phys. Chem. Chem. Phys* **2014**, *16*, 4740.